Springer Series in Materials Science 261

Adrian Crisan *Editor*

Vortices and Nanostructured Superconductors

Springer

Springer Series in Materials Science

Volume 261

The Springer Series in Materials Science covers the complete spectrum of materials physics, including fundamental principles, physical properties, materials theory and design. Recognizing the increasing importance of materials science in future device technologies, the book titles in this series reflect the state-of-the-art in understanding and controlling the structure and properties of all important classes of materials.

More information about this series at http://www.springer.com/series/856

Adrian Crisan
Editor

Vortices and Nanostructured Superconductors

Springer

Editor
Adrian Crisan
National Institute of Materials Physics
Magurele
Romania

ISSN 0933-033X ISSN 2196-2812 (electronic)
Springer Series in Materials Science
ISBN 978-3-319-59353-1 ISBN 978-3-319-59355-5 (eBook)
DOI 10.1007/978-3-319-59355-5

Library of Congress Control Number: 2017941475

Printed on acid-free paper

This Springer imprint is published by Springer Nature
The registered company is Springer International Publishing AG
The registered company address is: Gewerbestrasse 11, 6330 Cham, Switzerland

Preface

Starting with the success in liquefying He and the surprising discovery of the superconductivity of Hg by the group in Leiden led by H. Kammerling-Onnes, the last century provided us with the conceptual framework to understand and handle macroscopic quantum coherence: "superconductivity" in the case of existence of charge carriers, or "superfluidity" in the absence of charge carriers. No less than nine Nobel Prizes have been awarded for breakthrough discoveries and theories relating to superconductivity and superfluidity, from Kammerling-Onnes's initial 1913 prize, to the 2016 prize awarded to Thouless, Haldane and Kosterlitz for their theoretical discoveries of topological phases of matter and topological phase transitions, including topologically driven superconductivity.

Superconductivity is now an established (although, in some cases, not yet fully understood) form of macroscopic quantum coherence that regularly impacts the scientific community with new surprises, such as the discovery of high-temperature superconductivity in cuprates (Bednorz and Müller, IBM Zürich, Nobel Prize in 1987) followed rapidly by the discovery of superconductivity above the boiling point of nitrogen in $YBa_2Cu_3O_{7-x}$ by the Houston group of P. Chu; the discovery of superconductivity at 40 K in MgB_2; and later on, superconductivity in chalcogenides and pnictides, the last examples also being multi-component (multi-gap) superconductors. Superconductivity is a solid-state phenomenon that possesses the advantages that made electronic and semiconductor technology so successful: scalability and large-scale production. At the same time, radically different functionalities emerge due to macroscopic quantum coherence, from large-scale, energy-efficient applications due to electric current transportation without losses, to quantum computing and rapid single flux quantum electronics.

In this context, magnetic flux quanta in superconductors, also named "vortices" due to the circulating supercurrent supporting them, play crucial roles in both cases: (i) in superconducting electronics, they are the "carriers" of information instead of electrons; and (ii) in large-scale power applications, their mobility due to the Lorentz force leads to unwanted energy dissipation. So, for significant market penetration of such large-scale applications of superconductors, "pinning" of vortices by nanoscale engineered defects is crucial.

This book provides expert coverage of some modern and novel aspects of the study of vortex matter, dynamics, and pinning in nanostructured and multi-component superconductors. Vortex matter in superconducting materials is a field of enormous beauty and intellectual challenge, which began with the theoretical prediction of vortices by A. Abrikosov (Nobel Laureate for Physics in 2003, sadly deceased on March 23, 2017, age 88). Vortices, vortex dynamics, and pinning are key features in many of today's human endeavors: from the huge superconducting accelerating magnets and detectors at the Large Hadron Collider at CERN Geneva, which opened new windows of knowledge on the universe, to the Tokamak fusion magnets that will be utilized at the International Thermonuclear Energy Reactor in Cadarache, to the tiny superconducting transceivers using rapid single flux quanta, which have opened a revolutionary means of communication.

In this book, leading researchers survey the most exciting and important recent developments. The book offers something for almost everybody interested in the field: experimental techniques to visualize vortices and study their dynamics, nanotechnologies for improving current-carrying capabilities in high applied magnetic fields, current anisotropy, second magnetization peak, and intuitive and theoretical aspects concerning the novelty and beauty of multi-component superconductivity.

Chapter 1 presents unpublished data regarding the detailed evolution of a vortex approaching pinning centers. Using scanning Hall probe microscopy, the authors have directly visualized, at a microscopic level, the interaction of a single quantum vortex with pinning centers. When few adjacent pinning centers are present, the vortex can be trapped by one of them, while the interaction of the vortex with the adjacent pinning centers can be tuned by varying superconducting characteristic lengths with temperature. It was found that when the vortex size is comparable to the distance between two pinning centers, the vortex deforms along the line connecting the pinning centers and the magnetic flux spreads by embracing both pinning centers, thus generating a magnetic dipole. In contrast, a vortex located on an isolated pinning center preserves its round shape up to temperatures close to the critical temperature. The experimental data are in a good agreement with theoretical simulations based on the time-dependent Ginzburg–Landau approach.

Thirty years after the discovery of high critical temperature superconductors, the large-scale application of second-generation superconducting coated conductors based on rare-earth cuprates ($RE\mathrm{Ba_2Cu_3O_{7-x}}$) is still waiting for a lower price in terms of \$/kA m. This can be achieved by increasing the critical current. For high-field applications, this is even more crucial because of very large Lorentz forces. Fortunately, nano-engineered artificial pinning centers can provide large pinning forces to counteract Lorentz forces. Chapter 2 is a comprehensive review of various materials and architectures used for nanostructured $RE\mathrm{Ba_2Cu_3O_{7-x}}$ films with artificial pinning centers (APCs). Several categories of APCs are described in terms of their dimensionality (nanorods, nanoparticles, nanolayers, segmented nanorods, and more), and experimental results are discussed under the framework of Ginzburg–Landau theory. Various results obtained by many groups worldwide

are presented and analyzed, with emphasis on outstanding pinning performance in a wide range of temperatures (4.2–77 K) and magnetic fields (1–30 T).

Energy resources are now a major issue in the global economy. It is obvious that fossil fuels will not last forever. In addition, changes to the climate due to increasing CO_2 emissions are now obvious. Fortunately, we are witnessing the first, tentative steps toward a clean, sustainable "hydrogen economy," so in the not-so-distant future we would expect that liquid hydrogen with its boiling point of 20.3 K will be a common, abundant, and cheap liquid. In these circumstances, energy-efficient cryo-magnetic devices and equipment (transformers, magnets, motors, induction furnaces, superconducting-magnet energy storage, fault-current limiters, etc.) based on MgB_2 (a cheap and abundant superconductor with critical temperature of 40 K) cooled by liquid H will have a performance/price ratio much better than similar equipment based on copper wires, will require much less energy to operate, and will be more environmentally friendly. Tuning electronic structure and nanostructure is the critical issue for engineering an MgB_2 superconductor toward applications. In Chap. 3, a variety of chemical and microstructural control techniques that have been developed to artificially enhance flux pinning strength in the material are presented. The influence of chemical additives and oxygen doping on the formation of nanoprecipitates and superconducting properties, carbon doping effects, and methods of introducing carbon using different sources and microstructural control via ball-milling and mechanical alloying techniques are reviewed and summarized.

As shown in Chaps. 2 and 3, with creative materials nano-engineering, researchers have been successful in improving critical currents over the field and temperature ranges relevant to applications. Intrinsic thermodynamic properties and the interaction between the magnetic vortices and the pinning landscape combine to determine how much current is supported. Due to both factors, the resultant critical currents generally vary with the angle of the imposed external field. Chapter 4 explores what is known about this current anisotropy, very important in superconducting devices in which various parts are exposed to magnetic fields of various orientations. The difficulty of this problem stems partially from having two sources of anisotropy: the anisotropy in the vortex cross section, arising from the intrinsic mass anisotropy of the carriers of the vortex current; and the anisotropy of the pinning centers themselves. The effects of these two factors are not easily separated. It is never possible to have a fully isotropic pinning landscape in an anisotropic superconductor. If the critical current (I_c) varies strongly with angle, this presents challenges for coil designers who must keep the coil within safe operating margins of I/I_c everywhere within the coil. An unpredictable or only weakly predictable I_c with field, field orientation, and temperature means exploiting the full capacity of these materials is compromised. The chapter summarizes the common methods to analyze the critical current anisotropy. Firstly, there are scaling methods, such as the Blatter scaling and other scaling approaches which are a modification of this approach. Secondly, there are more direct methods of calculating the expected response from defects, which examine the pinning forces on vortices from defects under certain assumptions, and finally, the author presents the vortex path model or

maximum entropy method, which is an information theory or statistical approach for extracting information from the field orientation dependence of critical current.

The strong nonlinear relation between the current density and the electric field, along with nonlocal interactions, determines the complex behavior of vortex matter, which also includes "catastrophic" phenomena like vortex avalanches. Chapter 5 presents a brief review of the experimental studies devoted to these unstable vortex patterns, starting from historical findings up to recent works, and focusing on the analysis of vortex avalanches by means of magneto-optical imaging (MOI). The MOI technique, based on either Kerr (in reflection) or Faraday (in transmission) effects, is a powerful tool for the visualization of magnetic field distribution and enables the observation of magnetic field distribution in real time, on the whole surface of the superconductor, with microscopic resolution. The dynamics and morphology of the vortex avalanches are reported in detail, along with theoretical efforts for understanding and modeling this complex phenomenon. It is shown that vortex avalanches are ubiquitously occurring in superconductors if certain conditions are satisfied; in particular, temperature, applied magnetic field, and applied field rate are of paramount importance for observing/avoiding these phenomena. Together with the interest in the fundamental behavior of vortex matter, the understanding of vortex avalanches is instrumental for assessing the limits of superconductor usage in power applications.

Chapter 6 is devoted to the change of magnetic hysteresis curves and of vortex dynamics in "self-nanostructured" $La_{2-x}Sr_xCuO_4$ single crystals (with charge and spin stripes), offering useful information about the nature of the second magnetization peak occurring for single crystal specimens with random pinning. By decreasing x, with the external magnetic field oriented perpendicular to the stripe plane, the second magnetization peak completely disappears in the doping domain of a well-developed static stripe structure ($x \sim 1/8$) and reappears for $x \leq 0.10$. This behavior follows the instability of the quasi-ordered vortex solid (the Bragg vortex glass, stable against dislocation formation) in the presence of static stripe order (as revealed using small-angle neutron scattering experiments), which is confirmed by the determined temperature variation of the normalized vortex-creep activation energy. The results support the scenario in which the second magnetization peak is generated by the pinning-induced disordering of the Bragg vortex glass in the dynamic conditions of magnetic measurements.

The last two chapters are devoted to multi-component superconductivity, which is a rather new and very "fashionable" quantum phenomenon in various superconducting materials: multi-band superconductors in which different superconducting gaps open in different Fermi surfaces, films engineered at the atomic scale to enter the quantum confined regime, multilayer, two-dimensional electron gases at oxide interfaces, and complex materials in which different electronic orbitals or different carriers participate in the formation of the superconducting condensate. The increased number of degrees of freedom of the multi-component superconducting wave function allows for quantum effects that are otherwise unattainable in single-component superconductors. Chapter 7 focuses on inter-band phase difference soliton, the fractionalization of the unit magnetic flux quantum, and frustration between quantum phases of multiple components. Taking into account the fluctuations in the inter-band

phase difference provides a bridge between superconducting multiband condensates and other multicomponent macroscopic quantum systems such as Bose–Einstein condensates with multiple components and particle physics systems governed by a non-Abelian gauge field. Chapter 8 is theory-focused, investigating various excitation modes in multi-gap superconductors. In particular, the Nambu–Goldstone mode, Leggett mode, and Higgs mode are important and play a key role in multi-gap superconductors. The multiple-phase invariance in a multi-gap system is partially or totally spontaneously broken in a superconductor. The dispersion relation and the mass formulas of these modes are evaluated by using the functional integral method. The broken multiple-phase invariance leads to a new quantum phase such as time-reversal symmetry breaking, the emergence of massless modes, and fractionally quantized-flux vortices.

Finally, apart from the colleagues, friends, and collaborators who contributed to this book, I am grateful to my many friends from the Vortex community (VORTEX 10th Jubilee Conference is held in September 2017 in Rhodes together with the 65th anniversary of its initiator, Prof. V.V. Moshchalkov). The birth and title of this book are related to the International Conference on Superconductivity and Magnetism organized by Prof. Ali Gencer (Ankara University) every even year since 2008. Together with my friend, Prof. M. Milosevic (Antwerpen University), I chaired and co-organized a session entitled "Vortices and Nanostructured Superconductors," which provided excellent, world-class contributions and vivid discussions among the very best people in the field. And last, but not least, my special thanks to Sara Kate Heukerott from Springer who proposed this endeavor to me.

Financial support from the Romanian Ministry of Research and Innovation through POC (European Regional Development Fund, Operational Fund Competitiveness) Project P-37_697 number 28/01.09.2016 is gratefully acknowledged. Various funding agencies supporting the research activities which led to the results reported are mentioned in each chapter.

Bucharest, Magurele, Romania Adrian Crisan

Contents

1 Vortex Deformation Close to a Pinning Center 1
Jun-Yi Ge, Joffre Gutierrez, Valadimir N. Gladilin, Jacques Tempere, Jozef T. Devreese and Victor V. Moshchalkov

2 Pinning-Engineered $YBa_2Cu_3O_x$ Thin Films 15
Paolo Mele, Adrian Crisan and Malik I. Adam

3 Chemically and Mechanically Engineered Flux Pinning for Enhanced Electromagnetic Properties of MgB_2 65
Soo Kien Chen, Minoru Maeda, Akiyasu Yamamoto and Shi Xue Dou

4 Critical Current Anisotropy in Relation to the Pinning Landscape 109
Nick J. Long

5 Vortex Avalanches in Superconductors Visualized by Magneto-Optical Imaging 133
Francesco Laviano

6 Behavior of the Second Magnetization Peak in Self-nanostructured $La_{2-x}Sr_xCuO_4$ Single Crystals 159
Lucica Miu, Alina M. Ionescu, Dana Miu, Ion Ivan and Adrian Crisan

7 Emergence of an Interband Phase Difference and Its Consequences in Multiband Superconductors 185
Yasumoto Tanaka

8 Fluctuation Modes in Multi-gap Superconductors 219
Takashi Yanagisawa

Author Index 255

Subject Index 257

Contributors

Malik I. Adam Department of Mechanical Engineering, University Tenaga Nasional, Kajang, Malaysia

Soo Kien Chen Department of Physics, Faculty of Science, Universiti Putra Malaysia, Serdang, Selangor, Malaysia

Adrian Crisan National Institute of Materials Physics, Bucharest, Magurele, Romania

Jozef T. Devreese Universiteit Antwerpen, Antwerpen, Belgium

Shi Xue Dou Institute for Superconducting & Electronic Materials, Australian Institute of Innovative Materials, University of Wollongong, Wollongong, NSW, Australia

Jun-Yi Ge KU Leuven, Leuven, Belgium

Valadimir N. Gladilin KU Leuven, Leuven, Belgium

Joffre Gutierrez KU Leuven, Leuven, Belgium

Alina M. Ionescu National Institute of Materials Physics, Bucharest, Magurele, Romania; Faculty of Physics, University of Bucharest, Bucharest, Romania

Ion Ivan National Institute of Materials Physics, Bucharest, Magurele, Romania

Francesco Laviano Department of Applied Science and Technology, Politecnico di Torino, Torino, Italy

Nick J. Long Robinson Research Institute, Victoria University of Wellington, Wellington, New Zealand

Minoru Maeda Department of Physics, College of Science and Technology, Nihon University, Tokyo, Japan

Paolo Mele Research Center for Environmentally Friendly Materials Engineering, Muroran Institute of Technology, Muroran, Hokkaido, Japan

Dana Miu National Institute of Laser, Plasma, and Radiation Physics, Bucharest, Magurele, Romania

Lucica Miu National Institute of Materials Physics, Bucharest, Magurele, Romania

Victor V. Moshchalkov KU Leuven, Leuven, Belgium

Yasumoto Tanaka National Institute of Advanced Industrial Science and Technology, Tsukuba, Ibaraki, Japan

Jacques Tempere Universiteit Antwerpen, Antwerpen, Belgium

Akiyasu Yamamoto Department of Applied Physics, Tokyo University of Agriculture and Technology, Koganei, Tokyo, Japan

Takashi Yanagisawa Electronics and Photonics Research Institute, National Institute of Advanced Industrial Science and Technology, Tsukuba, Ibaraki, Japan

Chapter 1
Vortex Deformation Close to a Pinning Center

Jun-Yi Ge, Joffre Gutierrez, Valadimir N. Gladilin, Jacques Tempere, Jozef T. Devreese and Victor V. Moshchalkov

1.1 Introduction

In type-II superconductors, above the lower critical field H_{c1}, magnetic field penetrates into the superconductors in the form of quantized vortices with flux $\Phi_0 = h/2e$ (h, Plank constant; e, electron charge), forming the Abrikosov vortex lattice. When a current is applied, the vortices experience a Lorentz force perpendicular to the applied current. Vortex motion under this force leads to energy dissipation that limits technological applications. One common way to solve the problem is by introducing pinning centers to the superconductors, such as lithographically formed well-controlled pinning sites [1–4], ion-irradiated point defects [5], grain boundaries [6], and nanostructured self-assembled non-superconducting phases [7–9]. In all the above cases, the local superconductivity at pinning centers is suppressed, thus making them energetically favorable for vortices to be located on. Therefore, the critical current, above which the dissipation appears due to the vortex motion, can be strongly enhanced.

The vortex–pinning effect has been widely studied by many methods, for example, transport measurements [10–12], ac susceptibility measurements [13–15], and dc magnetization measurements [4, 16, 17]. In the transport measurements, vortices, going through a serious of different dynamic regimes [18], are depinned at large enough current density. Theoretical calculations predict that the vortex core becomes elongated along the direction of motion [19]. In the ac susceptibility measurements, under an ac driving force, vortices oscillate around the pinning centers. The interaction between pinning and vortices is manifested a sudden drop of the temperature dependence of in-phase ac susceptibility and a dissipation peak of the

J.-Y. Ge · J. Gutierrez · V.N. Gladilin · V.V. Moshchalkov (✉)
KU Leuven, Celestijnenlaan 200D, 3001 Leuven, Belgium
e-mail: Victor.Moshchalkov@fys.kuleuven.be

J. Tempere · J.T. Devreese
Universiteit Antwerpen, Universiteitsplein 1, 2610 Antwerpen, Belgium

A. Crisan (ed.), *Vortices and Nanostructured Superconductors*, Springer Series in Materials Science 261, DOI 10.1007/978-3-319-59355-5_1

out-of-phase ac susceptibility. Various phenomena have been revealed by using ac susceptibility measurement, such as the order–disorder transition and the memory effect of vortex lattice [13]. Isothermal magnetization measurement has also been used to study the vortex–pinning interaction. From the MH curves, the critical current density can be deduced which is directly related to the pinning effect of the superconductor.

However, most of these effects, such as vortex creep [20] and thermally activated flux motion [21], are based on the macroscopic response of the whole vortex lattice to the external drive. At the same time, little attention has been paid to the study of the behavior of an individual vortex when interacting with a pinning potential. A close investigation of this behavior can help us to manipulate vortices at a microscopic level which is important for potential applications such as quantum computing [22] and vortex generators [23]. Using the Ginzburg-Landau (GL) theory, Priour et al. [24] calculated the vortex behavior when approaching a defect. They predicted that a string will develop from the vortex core and extend to the vicinity of the defect boundary, while simultaneously the supercurrents and associated magnetic flux spread out and engulf the pinning center. However, this process happens fast and the vortex will be quickly attracted to the pinning center location, making it extremely hard to access directly with the local probe techniques so far.

Here, we propose a way to solve this problem by using a pair of pinning potentials where one of them traps a vortex. By changing the characteristic lengths, ξ (coherence length) and λ (penetration depth), simply through varying temperature, we are able to modify the effective interaction between the pinned vortex and the other pinning center nearby. This allows us to directly image the interaction process between a vortex and a pinning center with scanning Hall probe microscopy (SHPM). We have found that, with increasing temperature, the vortex shape becomes elongated with magnetic flux spreading over the adjacent pinning potential, thus providing strong evidence to the "string effect." The results of theoretical simulations based on the time-dependent Ginzburg-Landau (TDGL) approach are in line with our experimental findings.

1.2 Experimental

Our experiment is carried out on a 200-nm-thick superconducting Pb film prepared by ultra-high-vacuum (UHV) e-beam evaporation on a Si/SiO_2 substrate . During the deposition, the substrate is cooled down to liquid nitrogen temperature to avoid the Pb clustering. On top of Pb, 5-nm-thick Ge layer is deposited to protect the sample surface from oxidation. The sample surface is checked by atom-force microscopy (AFM), and a roughness of 0.2 nm is found. The critical temperature $T_c = 7.3$ K is determined by the local ac susceptibility measurements with a superconducting transition width of 0.05 K, indicating high quality of the sample. The pinning centers in the sample are created during sample preparation, and they appear randomly distributed. The local magnetic-field distribution was mapped using a low-temperature

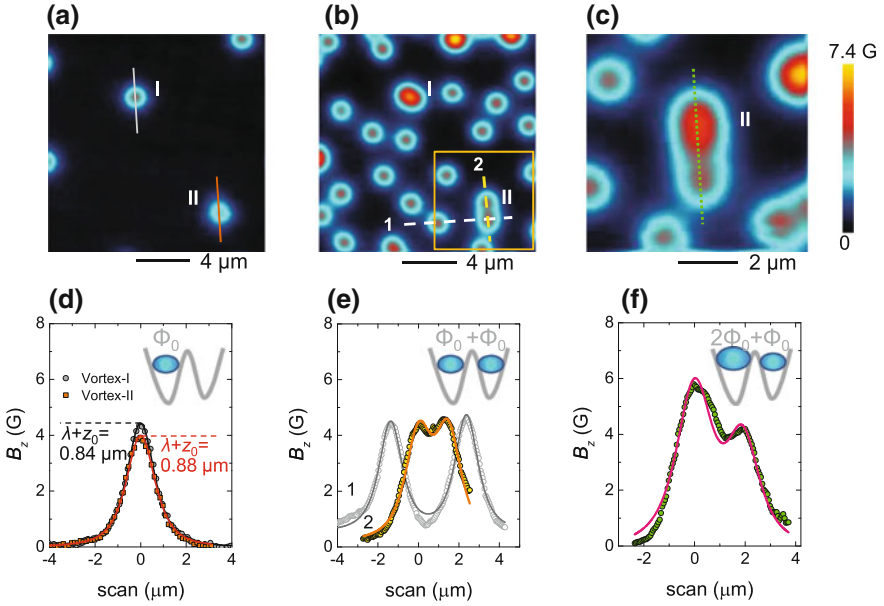

Fig. 1.1 Distribution of vortices after field cooling, revealing locations of pinning centers. **a**–**b**: FC images at $H = 0.3$ Oe (**a**), 2.4 Oe **b** and 3.6 Oe (**c**). **a** and **b** were taken at the same area, while **c** is taken at the area indicated by the square in (**b**). At *low* field (**a**), only single quantum vortices, sitting on the pinning centers, are observed. At relatively high fields (**b**) and (**c**), when all the pinning centers are occupied, pinned giant vortices with vorticity $L = 2$ and interstitial single quantum vortices appear. **d** Field profile along the cross section for the pinned vortices indicated by the *solid lines* in (**a**). **e** Field profiles along the *dashed lines* as shown in (**b**). **f** Vortex profile (symbols) along the dotted line in (**c**). The *solid lines* in panels **d**–**f** represent fitting of the data with the monopole model. The insets in **d**–**f** schematically show the pinned vortices at position II, with respect to the pinning landscape

SHPM from Nanomagnetics Instruments with a temperature stability better than 1 mK and magnetic-field resolution of 0.1 Oe. All the images are recorded in the lift-off mode by moving the Hall cross above the sample surface at a fixed height of ~0.7 μm. In all the measurements, the magnetic field is applied perpendicular to the sample surface.

1.2.1 Distribution of Pinning Centers

Figure 1.1 displays the vortex distributions at $T = 4.2$ K after field cooling (FC). It is well known that, in the presence of pinning, vortices will nucleate first at the pinning centers as shown in Fig. 1.1a. Two vortices, sitting at positions I and II, are observed in the scanned area. The field profiles for both vortices are displayed in Fig. 1.1d. It is shown that the field strength at the center of the vortex located at position I is higher

than that of vortex sitting at position II. To get quantitative information of confined magnetic flux and penetration depth, the monopole is used [25] with the following expression for the vortex-induced magnetic field:

$$B_z(r, z_0) = \frac{\boldsymbol{\Phi}}{2\pi} \frac{z_0 + \lambda}{\left[r^2 + \left(z_0 + \lambda\right)^2\right]^{3/2}} \tag{1.1}$$

where $\boldsymbol{\Phi}$ is the total flux carried by a vortex, λ is the penetration depth, and z_0 is the distance between effective two-dimensional electron gas (2DEG) of the Hall cross and the sample surface. The distance z_0 is constant in the used lift-off scanning mode. The fitting results are shown by solid lines in Fig. 1.1d, yielding $\boldsymbol{\Phi}_{\mathrm{I}} = \boldsymbol{\Phi}_{\mathrm{II}} = 1.1\boldsymbol{\Phi}_0$, $\lambda_{\mathrm{I}} + z_0 = 0.84\,\mu\mathrm{m}$ and $\lambda_{\mathrm{II}} + z_0 = 0.88\,\mu\mathrm{m}$. Since λ is related to the superfluid density, $\rho_s \propto \lambda^{-2}$ [26], the larger value of $\lambda_{\mathrm{II}} + z_0$, as compared to $\lambda_{\mathrm{I}} + z_0$, suggests a stronger suppression of superconducting condensate at the pinning site where vortex II is located.

The weakened superconductivity at the vortex-II position is further confirmed by the data of FC at a higher field as demonstrated in Fig. 1.1b. At position I, the field pattern in Fig. 1.1b apparently corresponds to a giant vortex with vorticity $L = 2$. On the other hand, around position II, two adjacent vortices are observed. The field profiles along the dashed lines in Fig. 1.1b are displayed in Fig. 1.1e. Both of them can be well fitted by two $\boldsymbol{\Phi}_0$-vortices located the distance of 3.7 μm (profile (1)) and 1.27 μm (profile (2)) from each other. The fitting results are shown by the solid lines. We also notice that in Fig. 1.1b, the distance between the two vortices located at position II is much smaller than that between interstitial vortices (indicated by the circles in Fig. 1.1b). All these observations suggest that there exist two adjacent pinning sites at the positions II. The pinning potentials of these sites force the two vortices to overcome the vortex–vortex repulsive interaction and stay close to each other. At even higher fields (Fig. 1.1c), one of the two adjacent pinning sites attracts two flux quanta as demonstrated by the field profiles in Fig. 1.1f. This may indicate that its pinning strength is stronger as compared to the bottom located pinning site.

1.2.1.1 Vortex Deformation with Temperature

Based on the above estimate of the relative pinning strength, now we focus on the effect of adjacent pinning potentials on a single vortex. To do this, we perform FC at 0.6 Oe to trap one $\boldsymbol{\Phi}_0$-vortex (vortex located at position II in Fig. 1.2a). When warming up the sample, both $\xi(T)$ and $\lambda(T)$ increase as compared to the temperature-independent distance between the two adjacent pinning sites. In other words, a vortex pinned to one of these sites effectively "approaches" the neighboring site. Each step of this process is imaged directly by SHPM as displayed in Fig. 1.2a–f. For comparison, the field of the vortex located at position I, trapped by an isolated pinning center, is also recorded and analyzed.

At low temperature, both vortices exhibit a circular shape, suggesting the supercurrents are localized about the vortex core. With increasing temperature, the vor-

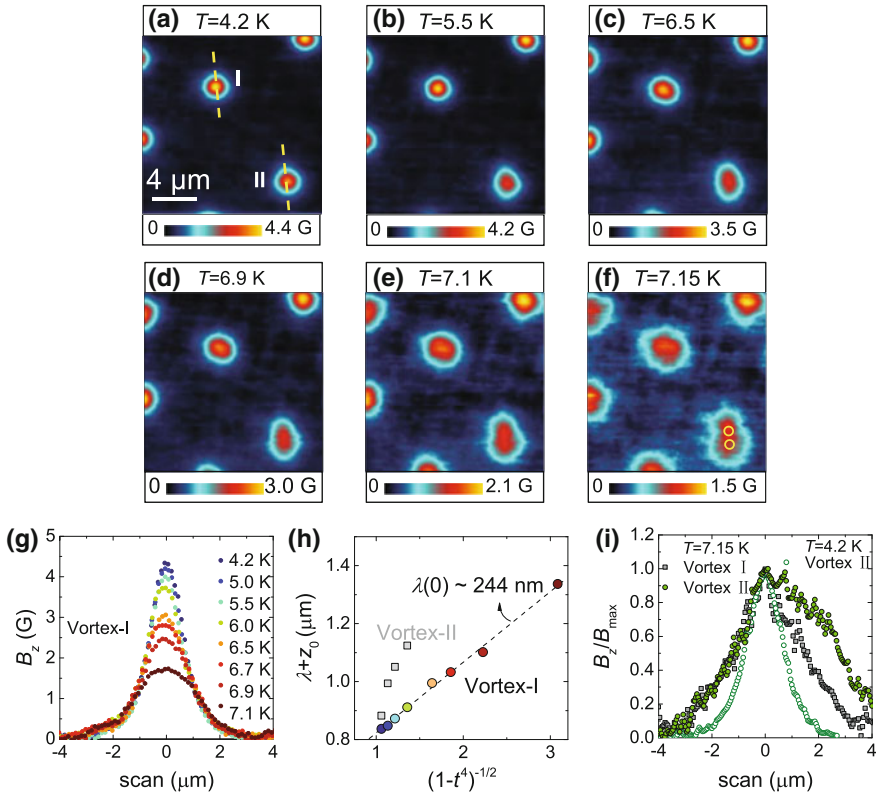

Fig. 1.2 (Color online) Vortex deformation observed at the pinning centers. **a**–**f** Scanning Hall probe microscopy images measured after first performing field cooling down to 4.2 K (**a**) and then increasing temperature to 5.5 K **b**, 6.5 K **c**, 6.9 K (**d**), 7.1 K **e** and 7.15 K (**f**). The circles in **f** indicate the locations where the two Φ_0-vortices are pinned in the FC image of Fig. 1.1b. **g** Field profiles of vortexI at different temperatures along the dashed lines indicated in (**a**). **h** $\lambda + z_0$ as a function of reduced temperature for vortex I (*squares*) and II (*circles*). The *dashed line* is a linear fit to the data. (I) Normalized field profiles for vortex II at 4.2 K (open *circles*) and 7.15 K (*filled circles*). For comparison, the field profile of vortex-I at 7.15 K (*squares*) is also shown

tex at position I preserves its circular shape up to 7.15 K, while the field strength decreases due to the magnetic profile broadening (Fig. 1.2g), correlated with an increase in the penetration depth. By fitting the profiles with the monopole of (1.1), the value of $\lambda(T) + z_0$ is extracted for different temperatures. According to the two-fluid model [27], in a superconductor with an isotropic energy gap, the temperature dependence of the penetration depth follows the expression $\lambda(T) = \lambda(0)/\sqrt{1-t^4}$, where $\lambda(0)$ is the zero temperature penetration depth and the reduced temperature is $t = T/T_c$. As shown by the circles in Fig. 1.2h, for vortex at position I the linear dependence of λ on $(1-t^4)^{-1/2}$ is obeyed, yielding $\lambda(0) \approx 244$ nm from the slope. However, the corresponding plot for the vortex located at position II (squares in Fig. 1.2h) fails to follow a linear dependence. This is mainly due to a vortex defor-

mation so that the monopole model cannot adequately describe the field distribution. As demonstrated in Figs. 1.2a–f, for vortex at position II, the broadening of the field profile with increasing temperature is asymmetric. As shown in Fig. 1.2i, the vortex field profile becomes elongated in the direction of the line connecting the two adjacent pinning centers (indicated by the open circles in Fig. 1.2f). The fact that this deformation only happens at high temperatures is in agreement with the prediction of [24]: There exists a temperature-dependent critical distance d_c between a vortex and a pinning center for the "string effect" to happen.

1.2.1.2 Simulation Results

To further analyze the observed phenomena, we performed simulations using the time-dependent Ginzburg-Landau (TDGL) equations (see, e.g., [26]). In our model, pinning centers in a superconducting film correspond to reduced local values of the mean free path l. In the case of inhomogeneous mean free path, the TDGL equation for the order parameter ψ can be written as follows:

$$\left(\frac{\partial}{\partial\tau}+i\varphi\right)\psi = \frac{l}{l_m}(\nabla - i\mathbf{A})^2\psi + 2(1-t)\left(1-\frac{l_m}{l}|\psi|^2\right)\psi, \tag{1.2}$$

where φ and $\mathbf{A}$ are the scalar and vector potentials, respectively, and l_m is the mean free path value outside the pinning centers. The relevant quantities are made dimensionless by expressing lengths in units of $\sqrt{2}\xi(0)$, time in units of $\pi\hbar/(4k_BT_c) \approx 11.6\tau_{GL}(0)$, magnetic field in units of $\Phi_0/(4\pi\xi^2(0)) = H_{c2}(0)/2$, scalar potential in units of $2k_BT_c/(\pi e)$, and ψ in units of $|\psi_\infty|$, the order parameter magnitude far away from pinning centers at $H = 0$. Here, μ_0 is the vacuum permeability, τ_{GL} is the Ginzburg-Landau time, and $\xi(0)$ is the coherence length outside the pinning centers at zero temperature.

The vector potential $\mathbf{A}$, for which we choose the gauge $\nabla\cdot\mathbf{A} = 0$, can be represented as $\mathbf{A} = \mathbf{A}_e + \mathbf{A}_s$. Here, $\mathbf{A}_e$ denotes the vector potential corresponding to the externally applied magnetic field $\mathbf{H}$, while $\mathbf{A}_s$ describes the magnetic fields induced by the currents $\mathbf{j}$, which flow in the superconductor:

$$\mathbf{A}_s(\mathbf{r}) = \frac{1}{2\pi\kappa^2}\int d^3r'\,\frac{\mathbf{j}(\mathbf{r}')}{|\mathbf{r}-\mathbf{r}'|}, \tag{1.3}$$

where $\kappa = \lambda/\xi$ is the Ginzburg-Landau parameter and the current density is expressed in units of $\Phi_0/[2\sqrt{2}\pi\mu_0\lambda(0)^2\xi(0)] = 3\sqrt{3}/(2\sqrt{2})j_c(0)$ with j_c, the critical (depairing) current density of a thin wire or film [26]. Integration in (1.3) is performed over the volume of the superconductor.

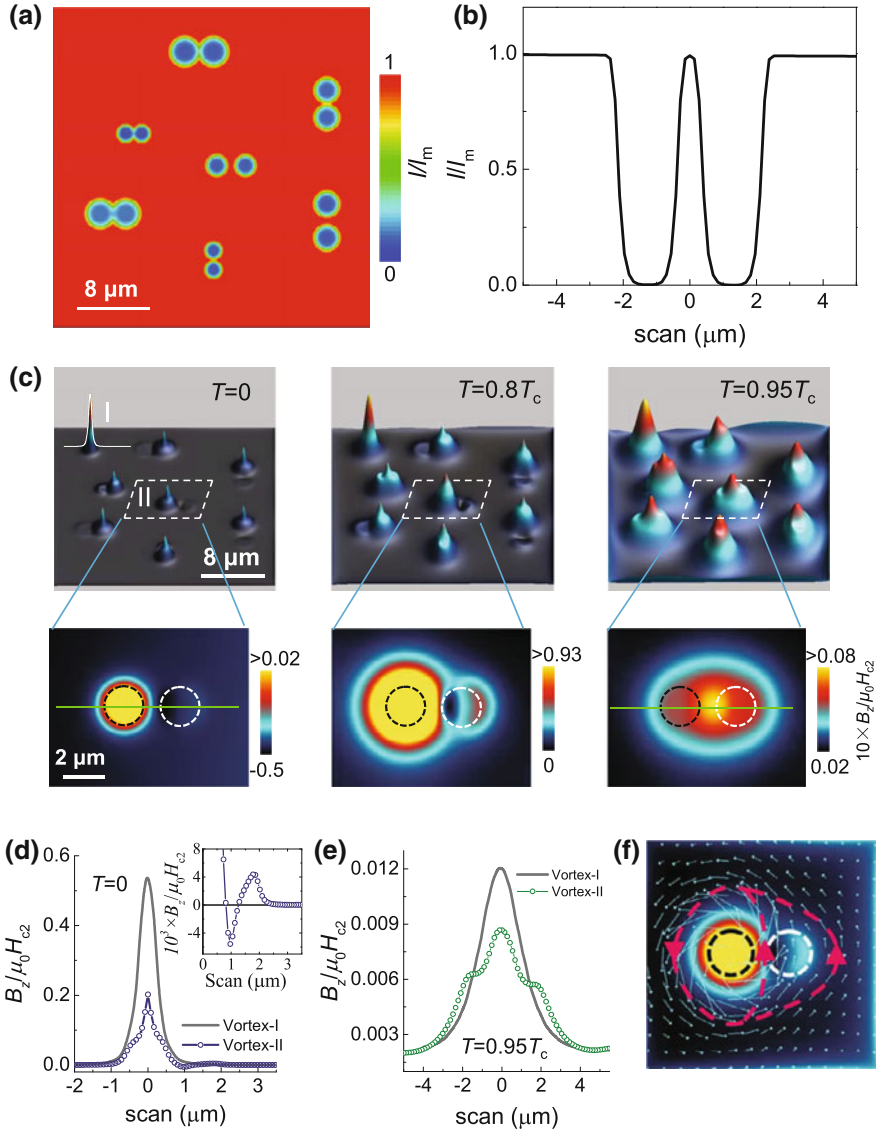

Fig. 1.3 (Color online) Simulation results. **a** Variations of the normalized mean free path in a $28 \times 28\,\mu\text{m}^2$ superconductor containing seven symmetric pairs of pinning centers with different sizes and strength. **b** Line profile of one pinning pair showing the variation of the normalized mean free path. **c** 3D view of magnetic-field patterns, corresponding to different values of progressively increasing temperature after field cooling to $T = 0$ at $H = 0.00375H_{c2}$. Seven pinned Φ_0 vortices and one interstitial vortex **i** are observed. The lower panels display an enlarged "top view" of the area indicated by the rectangles in each image. The dashed circles schematically show the pinning centers. The vortex field profiles along the direction of solid lines in **c** at $T = 0$ and $0.95T_c$ are given in (**d**) and (**e**), respectively. The inset in panel **d** provides a close view of the field profile for vortex II in the region between the two pinning centers. **f** Current density vector distribution for a vortex sitting on one pinning center of a pinning pair is indicated by the circles. The red dashed lines and the arrows show schematically the flow of vortex current around the pinning pair

In general, the total current density contains both the superconducting and normal components: $\mathbf{j} = \mathbf{j}_s + \mathbf{j}_n$ with

$$\mathbf{j}_s = (1-t)\left[\mathrm{Im}\left(\psi^* \nabla \psi\right) - \mathbf{A}|\psi|^2\right], \tag{1.4}$$

$$\mathbf{j}_n = -\frac{\sigma}{2}\left(\nabla\varphi + \frac{\partial \mathbf{A}}{\partial t}\right), \tag{1.5}$$

where σ is the normal-state conductivity, which is taken as $\sigma = 1/12$ in our units [28]. The distribution of the scalar potential φ is determined from the condition

$$\nabla \cdot \mathbf{j} = 0, \tag{1.6}$$

which reflects the continuity of currents in the superconductor. Both j_n and φ vanish when approaching (meta)stable states, which are of our main interest here.

We assume that the thickness of the superconductor film is sufficiently small, so that variations of the order parameter magnitude across the sample as well as currents in the this direction are negligible and (1.2) becomes effectively two-dimensional. This equation, together with (1.3) and (1.6), is solved self-consistently following the numerical approach described in [29]. Below, we consider a superconducting square with thickness of 200 nm, lateral sizes $X \times Y = 20\,\mu\mathrm{m} \times 20\,\mu\mathrm{m}$, $\xi(0) = 210\,\mathrm{nm}$, and $\lambda(0) = 160\,\mathrm{nm}$. As shown in Fig. 1.3A, the pinning sites are introduced as circular areas, where the mean free path l is smaller than its value l_m outside pinning centers. These pinning sites are arranged to form seven symmetric "pinning pairs" with different size/depth of pinning centers and distances between them.

The calculated vortex shape evolution with increasing temperature is displayed in Fig. 1.3c. After field cooling down to $T = 0$, a $\boldsymbol{\Phi}_0$ vortex is trapped by one of the pinning centers of each pinning pair. Remarkably, the distribution of the magnetic field, induced by such a pinned vortex, exhibits a tail toward the neighboring pinning center. In contrast, the interstitial vortex, marked as I, remains circularly symmetric up to T_c. The field distribution in the vicinity of pinned vortex-II at different temperatures is plotted as a color map below each image. The dashed circles indicate the positions of the two pinning centers, which form the pinning pair. At $T = 0$, while most of the flux is accumulated around one pinning center (black circle), a "magnetic-field dipole" appears at the position of the other pinning center (white circle). This can also be seen from the magnetic profiles (Fig. 1.3d), which are taken along the solid lines drawn in Fig. 1.3c (for comparison, the vortex profile for vortex-I is also shown). From the inset to Fig. 1.3d, a field dip between the two pinning centers is clearly seen.

The aforementioned magnetic-field dipole is reminiscent of what we have reported for the Meissner state of a superconductor [30]. When the Meissner currents flows through an area containing a pinning center, they generate in its vicinity two opposite sense current half-loops. The magnetic-field pattern, induced by this current configuration, has a dipole-like form (see Fig. 1.4a), which can be considered as a bound

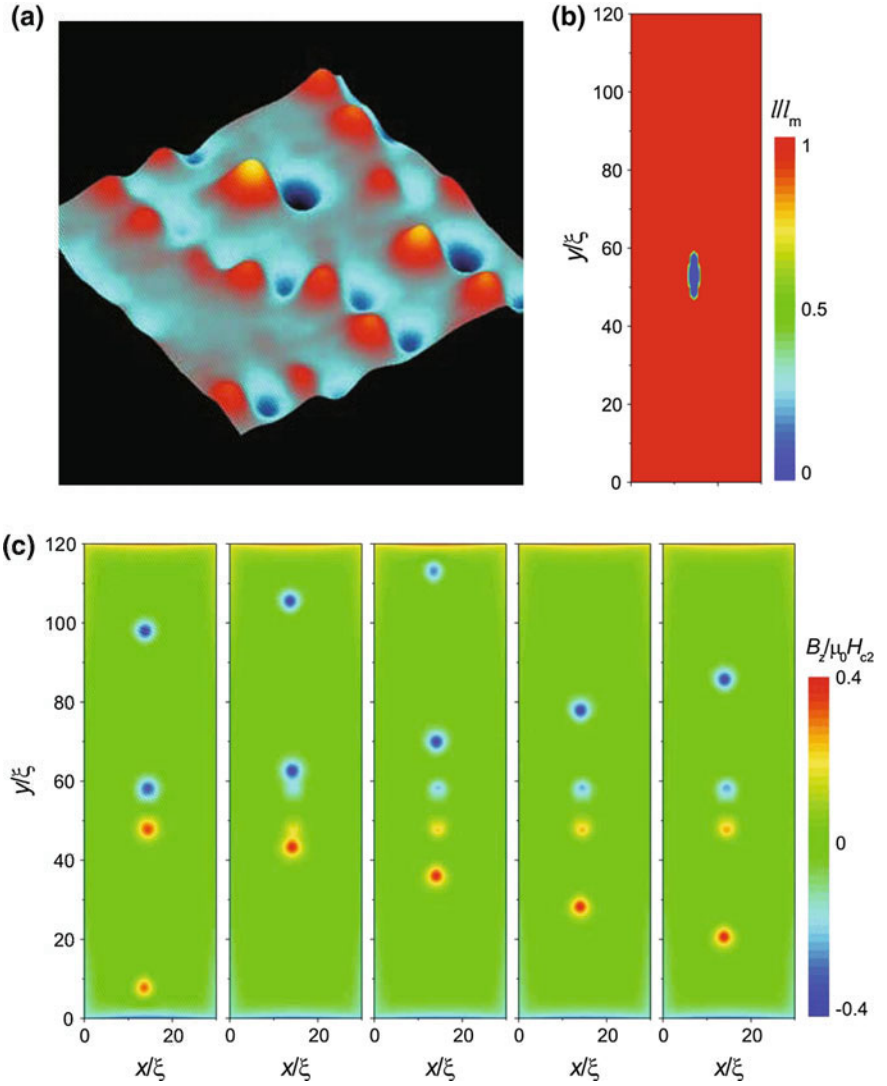

Fig. 1.4 (Color online) **a** Vortex dipoles observed in the Meissner state of a superconducting Pb film with naturally formed pinning centers. The *bright red* (*dark blue*) color indicates high (*low*) magnetic field. **b** Variations of the mean free path l assumed for simulation in a superconductor with one pinning center of elongated shape. (**c**) Simulated magnetic-field distributions for the pinning configuration in B, taken with the time step $\Delta tau = 5$. Single quantum vortices and antivortices are generated from the pinning center at large enough external current ($j_e = 0.55 j_c(T)$), applied in the x direction. The simulations are performed for the penetration depth $\lambda = \xi$ and the thickness $d = \xi$, where ξ is the coherence length. No external magnetic field is applied

vortex–antivortex pair. Such a bound vortex dipole is qualitatively different from the vortex–antivortex pairs usually observed in the mixed state of a type-II superconductor. Thus, the magnetic flux corresponding to either pole of a vortex dipole is not quantized: It is proportional to the local density of the Meissner currents and hence to the strength of the applied magnetic field. At the same time, our theoretical calculations show that, depending on the size and shape of a pinning center, bound vortex dipoles may evolve into spatially separated vortices and antivortices, if the current density flowing nearby the pinning site is sufficiently high (see Fig. 1.4b and c). In that sense, bound vortex dipoles may be considered as precursors of fully developed vortex–antivortex pairs, in which a vortex (antivortex) carries just one flux quantum. From the point of view of possible applications, measurements of bound vortex dipoles can provide a convenient way to detect hidden submicron defects in superconducting materials in a noninvasive way, which is rather difficult by using a conventional X-ray method.

While in [30] the magnetic-field dipoles are generated by the Meissner current flowing around regions with weakened superconductivity, here the vortex current plays the same role. The origin of the described magnetic-field patterns can be easily understood from Fig. 1.3f, which shows the current density vector distribution for a vortex trapped by one of the sites of the pinning pair. The vortex current extends to engulf both pinning centers of the pair as indicated by the arrows, while between the two pinning centers the current density is reduced. Such a current distribution leads to the formation of a dipole-like pattern of the magnetic field at the location of the unoccupied pinning site.

When increasing temperatures, the circulating currents of the vortex spread over a larger area due to an increase of λ. As a result, the supercurrent flowing around the unoccupied pinning center becomes stronger and the "magnetic-field dipole" signal is enhanced. However, due to the limited resolution of our experimental technique, a negative field signal between the two pinning centers is rather difficult to detect. At even higher temperatures ($T \geq 0.95T_c$), when the vortex core size, which is $\sim\xi$, becomes comparable to or larger than the size of the pinning pair as a whole, the thermodynamically stable state corresponds to a vortex centered between the pinning sites (see Fig. 1.3e): Just this position of the vortex provides the maximum overlap of the vortex core with the pinning sites. In this case, the pinning pair acts as a single pinning site with strongly anisotropic shape, which leads to an elongated magnetic-field pattern for the pinned vortex. Similar pinning geometry conversion has also been suggested in Refs. [31, 32]. We have also simulated the vortex deformations in the case of asymmetric pinning pairs, which lead to qualitatively similar results (not shown here).

The vortex distributions at relatively high magnetic fields are shown in Fig. 1.5. At those fields, a pinning center can accommodate more than one vortex. This is consistent with what we have observed in Fig. 1.1b. However, instead of giant vortices, which may be presumed from the experimental data, vortex clusters are formed at pinning sites considered in our theoretical model. This resembles the effect observed in superconducting film with blind antidots, where, due to the large size of blind holes, the trapped $n\Phi_0$ multiquanta vortex at the antidot dissociates into n individual

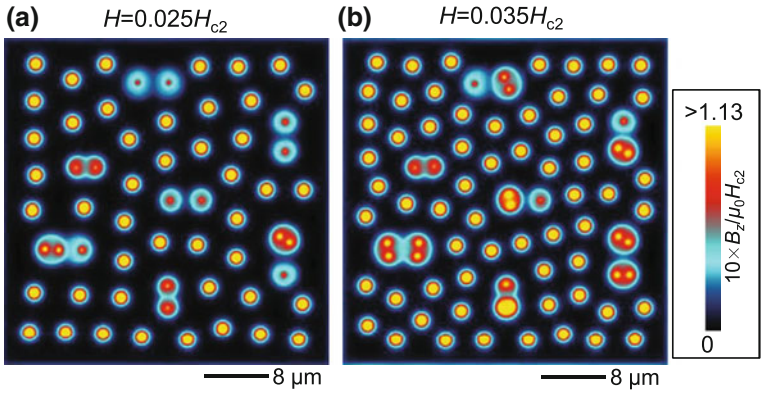

Fig. 1.5 (Color online) Vortex patterns at relatively high magnetic fields. **a** Vortex patterns, corresponding to FC, for the pinning landscapes of Fig. 1.3a at $H = 0.025H_c$ **a** and $0.035H_{c2}$ (**b**)

Φ_0 vortices in the bottom superconducting layer [33]. In this connection, it seems worth mentioning that at present, the resolution of our experimental technique may be not sufficient to confidently distinguish between giant vortices and compact vortex clusters.

To summarize, we have performed both experimental and theoretical studies of vortex states in the vicinity of a pinning center. Our experimental work provides clear evidence of vortex deformation by a nearby pinning center, where the vortex supercurrents and the induced magnetic-field profile expand and engulf the pinning site. The results of our TDGL theoretical modeling, which are fully consistent with the experimental observations, reveal an additional fine structure ("magnetic-field dipoles") in the magnetic field patterns, induced by those deformed vortices. By simply varying the temperature, the vortex geometry can be well controlled. A detailed understanding of vortex deformation by adjacent pinning centers paves the way to manipulate the vortex current distributions at a microscopic level. This provides new possibilities to control single flux quanta in superconducting devices.

Acknowledgements We acknowledge the support from FWO and the Methusalem funding by the Flemish government. This work is also supported by the MP1201 COST action. This research was also supported by the Flemish Research Foundation (FWO-Vl), project nrs. G.0115.12N, G.0119.12N, G.0122.12N, G.0429.15N and by the Research Fund of the University of Antwerpen.

References

1. M. Baert, V.V. Metlushko, R. Jonckheere, V.V. Moshchalkov, Y. Bruynseraede, Composite flux-line lattices stabilized in superconducting films by a regular array of artificial defects. Phys. Rev. Lett. **74**, 3269 (1995)

2. V.V. Moshchalkov, M. Baert, V.V. Metlushko, E. Rosseel, M.J. Van Bael, K. Temst, Y. Bruynseraede, R. Jonckheere, Pinning by an antidot lattice The problem of the optimum antidot size. Phys. Rev. B **57**, 3615 (1998)
3. N. Haberkorn, B. Maiorov, I.O. Usov, M. Weigand, W. Hirata, S. Miyasaka, S. Tajima, N. Chikumoto, K. Tanabe, L. Civale, Influence of random point defects introduced by proton irradiation on critical current density and vortex dynamics of Ba(Fe0.925Co0.075)2As2 single crystals. Phys. Rev. B **85**, 014522 (2012)
4. D. Ray, C.J. Olson Reichhardt, B. Jank, C. Reichhardt, Strongly enhanced pinning of magnetic vortices in type-II superconductors by conformal crystal arrays. Phys. Rev. Lett. **110**, 267001 (2013)
5. B.M. Vlcek, H.K. Viswanathan, M.C. Frischherz, S. Fleshler, K. Vandervoort, J. Downey, U. Welp, M.A. Kirk, G.W. Crabtree, Role of point defects and their clusters for flux pinning as determined from irradiation and annealing experiments in YBa2Cu3O7-δ single crystals. Phys. Rev. B **48**, 4067 (1993)
6. C.-L. Song, Y.-L. Wang, Y.-P. Jiang, L. Wang, K. He, X. Chen, J.E. Hokman, X.-C. Ma, Q.-K. Xue, Suppression of Superconductivity by Twin Boundaries in FeSe. Phys. Rev. Lett. **109**, 137004 (2012)
7. J.L. MacManus-Driscoll, S.R. Foltyn, Q.X. Jia, H. Wang, A. Serquis, L. Civale, B. Maiorov, M.E. Hawley, M.P. Maley, D.E. Peterson, Strongly enhanced current densities in superconducting coated conductors of $YBa_2Cu_3O_{7-x} + BaZrO_3$. Nat. Mater. **3**, 439–443 (2004)
8. J. Gutierrez, A. Llordes, J. Gazquez, M. Gibert, N. Roma, S. Ricart, A. Pomar, F. Sandiumenge, N. Mestres, T. Puig, X. Obradors, Strong isotropic flux pinning in solution-derived $YBa_2Cu_3O_{7-x}$ nanocomposite superconductor films. Nat. Mater. **6**, 367–373 (2007)
9. S.R. Foltyn, L. Civale, J.L. MacManus-Driscoll, Q.X. Jia, B. Maiorov, H. Wang, M. Maley, Materials science challenges for high-temperature superconducting wire. Nat. Mater. **6**, 631–642 (2007)
10. J. Ge, S. Cao, S. Shen, S. Yuan, B. Kang, J. Zhang, Superconducting properties of highly oriented Fe 1.03 Te 0.55 Se 0.45 with excess Fe. Solid State Commun. **150**, 1641 (2010)
11. D.B. Rosenstein, I. Shapiro, B.Y. Shapiro, HTransport current carrying superconducting film with periodic pinning array under strong magnetic fields. Phys. Rev. B **83**, 064512 (2011)
12. I. Sochnikov, A. Shaulov,Y. Yeshurun, G. Logvenov, I. Bozovic, Large oscillations of the magnetoresistance in nanopatterned high-temperature superconducting films. Nat. Nanotech. **5**, 516C519 (2010)
13. J. Ge, J. Gutierrez, J. Li, J. Yuan, H.-B. Wang, K. Yamaura, E. Takayama-Muromachi, V.V. Moshchalkov, Peak effect in optimally doped p-type single-crystal $Ba_{0.5}K_{0.5}Fe_2As_2$ studied by ac magnetization measurements. Phys. Rev. B **88**, 144505 (2013)
14. J. Ge, J. Gutierrez, M. Li, J. Zhang, V.V. Moshchalkov, Vortex phase transition and isotropic flux dynamics in $K_{0.8}Fe_2Se_2$ single crystal lightly doped with Mn. Appl. Phys. Lett. **103**, 052602 (2013)
15. J. Ge, J. Gutierrez, J. Li, J. Yuan, H.-B. Wang, K. Yamaura, E. Takayama-Muromachi, V.V. Moshchalkov, Dependence of the flux-creep activation energy on current density and magnetic field for a $Ca_{10}(Pt_3As_8)[(Fe_{1-x}Pt_x)_2As_2]_5$ single crystal. Appl. Phys. Lett. **104**, 112603 (2014)
16. Y.L. Wang, X.L. Wu, C.-C. Chen, C.M. Lieber, Enhancement of the critical current density in single-crystal Bi2Sr2CaCu208 superconductors by chemically induced disorder. Proc. Natl. Acad. Sci. USA **87**, 7058–7060 (1990)
17. M. Motta, F. Colauto, W. Ortiz, J. Fritzsche, J. Cuppens, W. Gillijns, V. Moshchalkov, T. Johansen, A. Sanchez, A. Silhanek, Enhanced pinning in superconducting thin films with graded pinning landscapes. Appl. Phys. Lett. **102**, 212601 (2013)
18. J. Gutierrez, A.V. Silhanek, J. Van de Vondel, W. Gillijns, V.V. Moshchalkov, Transition from turbulent to nearly laminar vortex flow in superconductors with periodic pinning. Phys. Rev. B **80**, 104514 (2009)
19. D.Y. Vodolazov, F.M. Peeters, Rearrangement of the vortex lattice due to instabilities of vortex flow. Phys. Rev. B **76**, 014521 (2007)

20. T. Klein, H. Grasland, H. Cercellier, P. Toulemonde, C. Marcenat, Vortex creep down to 0.3 K in superconducting Fe(Te, Se) single crystals. Phys. Rev. B **89**, 014514 (2014)
21. L. Jiao, Y. Kohama, J.L. Zhang, H.D. Wang, B. Maiorov, F.F. Balakirev, Y. Chen, L.N. Wang, T. Shang, M.H. Fang, H.Q. Yuan, Upper critical field and thermally activated flux flow in single-crystalline $Tl_{0.58}Rb_{0.42}Fe_{1.72}Se_2$. Phys. Rev. B **85**, 064513 (2012)
22. O. Romero-Isart, C. Navau, A. Sanchez, P. Zoller, J.I. Cirac, Superconducting vortex lattices for ultracold atoms. Phys. Rev. Lett. **111**, 145304 (2013)
23. V.M. Fomin, R.O. Rezaev, O.G. Schmidt, Tunable generation of correlated vortices in open superconductor tubes. Nano Lett. **12**, 1282 (2012)
24. D. Priour Jr., H. Fertig, Deformation and depinning of superconducting vortices from artificial defects: a Ginzburg-Landau study. Phys. Rev. B **67**, 054504 (2003)
25. J. Ge, J. Gutierrez, J. Cuppens, V.V. Moshchalkov, Observation of single flux quantum vortices in the intermediate state of a type-I superconducting film. Phys. Rev. B **88**, 174503 (2013)
26. M. Tinkham, *Introduction to Superconductivity* (McGraw-Hill Inc, New York, 1996)
27. J. Bardeen, Two-fluid model of superconductivity. Phys. Rev. Lett. **1**, 399 (1958)
28. R. Kato, Y. Enomoto, S. Maekawa, Computer simulations of dynamics of flux lines in type-II superconductors. Phys. Rev. B **44**, 6916 (1991)
29. A.V. Silhanek, V.N. Gladilin, J. Van de Vondel, B. Raes, G.W. Ataklti, W. Gillijns, J. Tempere, J.T. Devreese, V.V. Moshchalkov, Local probing of the vortex-antivortex dynamics in superconductor/ferromagnet hybrid structures. Supercond. Sci. Technol. **24**, 024007 (2011)
30. J. Ge, J. Gutierrez, V.N. Gladilin, J.T. Deverese, V.V. Moshchalkov, Bound vortex dipoles generated at pinning centres by Meissner current. Nat. Commun. **6**, 6573 (2015)
31. J. Trastoy, M. Malnou, C. Ulysse, R. Bernard, N. Bergeal, G. Faini, J. Leseur, J. Briatico, J.E. Villegas, Freezing and thawing of artificial ice by thermal switching of geometric frustration in magentic flux lattices. Nat. Nanotech. **9**, 710–715 (2014)
32. M.L. Latimer, G.R. Berdiyorov, Z.L. Xiao, F.M. Peeters, W.K. Kwok, Realization of artificial Ice systems for magnetic vortices in a superconducting MoGe thin film with patterned nanostructures. Phys. Rev. Lett. **111**, 067001 (2013)
33. A. Bezryadin, Y.N. Ovchinnikov, B. Pannetier, Nucleation of vortices inside open and blind microholes. Phys. Rev. B **53**, 8553 (1996)

Chapter 2
Pinning-Engineered $YBa_2Cu_3O_x$ Thin Films

Paolo Mele, Adrian Crisan and Malik I. Adam

2.1 Introduction

In order to be used for practical applications such as lossless current transportation, winding of magnets, etc., superconducting materials should possess not only high enough critical temperature T_c, but also critical current density J_c, and upper critical field B_{c2} as large as possible to cover a wide range of the currently available and future technologies of superconductivity.

Introduction of nanosized artificial pinning centers (APCs) was widely used to strongly enhance J_c of high-temperature superconductor (HTSC) like $YBa_2Cu_3O_x$ (YBCO, $T_c = 92$ K) in magnetic field. Figure 2.1 shows the performance of state-of-the-art YBCO thin films with APCs in comparison with other superconducting materials [1]. It is worth noting the outstanding performance of APCs-added YBCO films at 77 K, surpassing the conventional superconducting metallic cables (NbTi, Nb_3Sn) at 4.2 K. The incorporation of one-dimensional defects such as nanorods in YBCO films prepared by pulsed laser deposition (PLD) could be exemplified as to how effective the APC technology evolves. After the pioneering work of J. McManus-Driscoll and coworkers on YBCO+BZO nanorods [2], in 2008 YBCO films added with 4 wt% BSO have been reported to

P. Mele (✉)
Research Center for Environmentally Friendly Materials Engineering, Muroran Institute of Technology, Muroran, Hokkaido, Japan
e-mail: pmele@mmm.muroran-it.ac.jp

A. Crisan
National Institute of Materials Physics, 077125 Bucharest, Magurele, Romania
e-mail: adrian.crisan@infim.ro; acrisan652@gmail.com

M.I. Adam
Department of Mechanical Engineering, University Tenaga Nasional, Kajang, Malaysia
e-mail: idriesm@uniten.edu.my; omavis1@gmail.com

A. Crisan (ed.), *Vortices and Nanostructured Superconductors*, Springer Series in Materials Science 261, DOI 10.1007/978-3-319-59355-5_2